Available online at www.sciencedirect.com
SCIENCE DIRECT®
Coordination Chemistry Reviews 249 (2005) 1986–1996
COORDINATION CHEMISTRY REVIEWS
www.elsevier.com/locate/ccr

Review

Thin films of transition metal-containing molecule-based materials: A highlight on electrochemically processed systems

Lydie Valade *, Dominique de Caro, Mario Basso-Bert, Isabelle Malfant, Christophe Faulmann, Bénédicte Garreau de Bonneval, Jean-Pierre Legros

Laboratoire de Chimie de Coordination, CNRS UPR8241, "Molécules et Matériaux", 205 Route de Narbonne, 31077 Toulouse Cedex 4, France

Received 29 October 2004; accepted 30 March 2005
Available online 24 May 2005

Contents

Abstract

Molecule-based materials show a large variety of physical properties such as conductivity, magnetism, optics, which render them attractive for a new generation of electronic devices. Electrochemical processing is one of the methods that may be applied to grow thin conductive films. Depending on the systems, the technique itself and the two-dimensional growth may afford new phases and/or similar or different properties

* Corresponding author. Tel.: +33 5 61 33 31 38; fax: +33 5 61 55 30 03.
E-mail address: valade@lcc-toulouse.fr (L. Valade).

0010-8545/$ – see front matter
doi:10.1016/j.ccr.2005.03.030

from those observed on single crystals. Several examples of compounds carrying dithiolato-, polyoxo- or cyano-ligands are provided and the particular use of silicon wafers as substrates is considered.

Keywords: Transition metal; Molecule-based material; Electrodeposition; Thin film; Silicon

1. Introduction

The miniaturization of components is an important goal in the electronic industry nowadays. Top down and bottom up approaches are being developed. The first one uses conventional inorganic materials while one of the interests of the second one is to organize atoms or molecules on surfaces. Among the second type, using single molecules, systems have been produced as nanoparticles, nanowires, thin films or monolayers [1–7]. Towards the goal of producing reliable components chemists must be able to produce materials showing electronic properties in the bulk, but also demonstrate the ability of these materials to be organized on surfaces, i.e. the feasibility step towards devices. If we consider purely organic molecular systems, work has proceeded much further than with metal–organic systems. Organic electronic components have already been incorporated into products such as organic light-emitting diodes (OLEDs) displays, thin film transistors (TFTs) or flexible electronic paper [8].

In order to process metal–organic molecule-based materials as thin films, various techniques may be applied [7]. The choice of technique depends mainly on the chemical properties of the precursors. Gas phase reactions involved in vacuum deposition or chemical vapor deposition (CVD) techniques imply the use of vaporizable precursors. In Langmuir–Blodgett (LB), dip coating, drop casting, spin coating, stamping or ink-jet printing techniques, the precursors are used in solution and therefore have to be soluble. Stability either in the gas phase or in solution is another requirement. The advantage of solution techniques versus gas phase ones is that they are performed at room temperature and allow for the use of a larger variety of substrates including polymers. Nevertheless, in the molecule-based materials domain, gas phase processing methods deal with much lower temperatures (typically <100 °C) than those applied for metallic or ceramic film growth (typically from 200 to 1400 °C). Moreover, in ultra high vacuum conditions, surfaces of high quality are obtained and therefore show a good suitability for in situ studies through nanoprobe techniques. For producing conductive thin films, electrodeposition is another available solution-based technique where an electrochemical activation of the precursor is necessary to afford the material.

Transition metal complexes have been widely used to afford molecule-based materials. They act as metal sources or as building blocks. When they act as a metal source, the material formation results from ligand exchange, as for example in the formation of members of the $M(TCNE)_2$ family, i.e. the magnets $V(TCNE)_2$, $Cr(TCNE)_2$, $Nb(TCNE)_2$ and $Mo(TCNE)_2$, obtained by CVD from TCNE (Fig. 1) and $V(C_6H_6)_2$ [9], $Cr(C_6H_6)_2$ [10], $Nb(iPr_2\text{-dad})_3$ (iPr_2-dad = 1,4-diisopropyl-1,4-diazabuta-1,3-diene) [11], and $Mo(C_6H_5CH_3)_2$ [12], respectively.

When transition metal complexes act as building blocks, their chemical composition remains unchanged through material formation, as for example the dithiolene complex $[Ni(dmit)_2]$ in the preparation of the superconductor $TTF[Ni(dmit)_2]_2$ [13,14]. Of the metallic conductors known to date, i.e. the metallic neutral single molecule system, $Ni(tmdt)_2$, is also a dithiolene complex [15]. Cp-dithiolenes complexes showing magnetic properties have been prepared [16]. Many conductive phases containing transition metal complexes associated with the TTF-like organic molecules have been isolated [17,18]. Complexes also provide magnetic properties to the final material either as a single property in magnets such as $[(Cp^*)_2Fe][TCNE]$

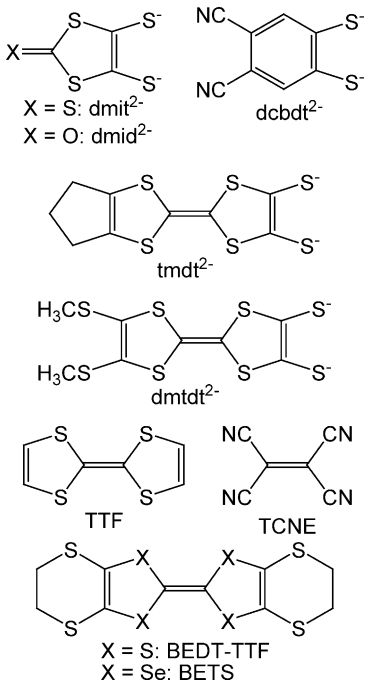

Fig. 1. Chemical structures and abbreviated usual names of dithiolate ligands and donor molecules. $dmit^{2-}$ = dimercaptoisotrithione or 1,3-dithio-2-thione-4,5-dithiolate; $dmid^{2-}$ = 1,3-dithio-2-one-4,5-dithiolate; $dcbdt^{2-}$ = 1,2-dicyano-benzene-4,5-dithiolate; $tmdt^{2-}$ = trimethylene-tetrathiafulvalene-dithiolate; $dmtdt^{2-}$ = dimethylthio-tetrathiafulvalene-dithiolate; TTF = tetrathiafulvalene; TCNE = tetracyanoethylene; BEDT-TTF = bis-ethylenedithio-tetrathiafulvalene; BETS = bis-ethylenedithio-tetraselenafulvalene.

[19] and $[(Cp^*)_2Mn][Ni(dmit)_2]$ [20] or as an associated one in magnetic conductors or superconductors [21,22] such as $(BEDT\text{-}TTF)_4(H_3O)[M(C_2O_4)_3],C_6H_5CN$ (M = Fe, Cr) [23], and $(BEDT\text{-}TTF)_3[MnCr(C_2O_4)_3],CH_2Cl_2$ [24], $(BETS)_x[MnCr(C_2O_4)_3]$, CH_2Cl_2 [25] or $(BETS)_2FeCl_4$ [26]. Other types of complexes such as the nitroprusside $[Fe(CN)_5NO]^{2-}$ building block, known to exhibit photochromic properties, have tentatively been associated with donor molecules to afford photochromic conductors [27–32]. The spin crossover (SCO) phenomenon, a property allowing bi-stability sometimes accompanied with a memory effect, has been observed in iron, chromium and manganese complexes [33–35]. Prussian blue and its analogues form another family of highly studied molecule-based magnetic materials containing transition metals. These materials exhibit various novel magnetic properties which have been summarized in recent reviews [36–38]. For example, $V[Cr(CN)_6]_{0.86}\cdot 2.8H_2O$ is a molecular magnet exhibiting a higher than room temperature T_c value (315 K) [39]. Although they differ from coordination-type complexes cited above, polyoxometalates (POMs) should also be mentioned. These inorganic species appear as counter-ions in conductive materials where the conductive part issues either from TTF-like donors or from polymers [40,41]. Transition metal dithiolenes form one of the largest existing families of building blocks used so far to prepare molecule-based conductors [42–44].

Electrocrystallization of molecule-based materials as single crystals has been reviewed [45]. Therefore, only thin film formation using the electrodeposition method is considered in this paper. Within the examples selected, the complex is either the oxidized species itself or acts as the counter-ion. In the latter case, it may afford an additional property. Transition metal complexes appearing as building blocks in single or multiproperty conductive, magnetic or photochromic materials are considered. Growth on various types of substrates is presented. The use of silicon wafers is singled out.

2. Experimental

2.1. Substrates

Film growth is governed by an electrochemical activation, and therefore conductive substrates must be used; many kinds have been applied. A platinum foil is used to grow films of the $(NBu_4)_{0.9}[Ni(dmid)_2]$ phase [46]. Use of a single-crystal Au(1 1 0) substrate is reported for growing epitaxial Prussian blue thin films [47]. A SnO_2 substrate [48], glassy carbon and highly oriented pyrolytic graphite [49] are used for the deposition of chromium analogues of Prussian blue. Gold electrodes evaporated on cadmium stearate pre-coated PET (polyethylene-terephthalate) substrates covered by an LB-film of $[(C_{10}H_{21})_3NCH_3][Au(dmtdt)_2]$ are applied for the electrochemical formation of the neutral conductor $[Au(dmtdt)_2]$ [50]. An earlier study shows the formation of LB-$[Au(dmit)_2]$ films also using evaporated gold electrodes, but on icosanoic acid pre-coated PET [51]. Copper substrates [52] and ITO (indium tin oxide) [53,54] anodes are used to grow deposits of neutral $M(dmit)_2$ material (M = Ni, Pd). Electronics is largely based on silicon technology. Therefore, we have considered the use of silicon(1 0 0) wafers as electrodes to grow the films. The conductivity of silicon covers a wide range of values depending on whether the material is doped or not. We perform electrolyses using intrinsic silicon, which is a low conductive type ($\sigma = 5 \times 10^{-3}$–$3 \times 10^{-3}$ S cm^{-1}) and p-type one. The entire silicon wafer (diameter 2 in., thickness 275 μm) or strips of it (3 cm × 0.5 cm) is used.

Cleaning procedures are applied before dipping the substrate in the electrolyte solution. Pt is immersed in a 2 mol L^{-1} NaOH aqueous solution, then rinsed with acid, water and finally acetonitrile [46]. Au substrates are electrochemically polished in a solution containing ethylene glycol, HCl and ethanol and annealed in a H_2 flame just before electrodeposition [47]. Si is cleaned in a NH_4F/HF solution (12.5% HF 50% and 87.5% NH_4F 40%) to remove the native oxide layer and then washed with distilled water and with the solvent used for electrodeposition. The cleaning procedures have two goals: removing impurities from the surface and etching the surface in order to improve the anchorage of the deposit. In the case of silicon substrates, the cleaning treatment can lead to a nanostructuration of the surface, an increase of its roughness, and an improvement of the adherence of the coatings. A Pt wire is typically used as counter electrode and saturated calomel electrode (SCE) or AgCl/Ag are the reference electrodes when potentiostatic electrolysis is applied.

2.2. Electrodeposition procedure

The substrate is used as the anode and galvanostatic or potentiostatic electrolysis is carried out using similar solutions of the precursors as in conventional electrocrystallization [45]. H-type cells are the more commonly used for galvanostatic electrolysis. One-compartment cells are also convenient, in particular when silicon wafers are used [55]. In this case, larger volumes (300 mL) of electrolyte solution are necessary relatively to H-type cells (10–20 mL). Taking advantage of a large volume of electrolyte and a large electrode surface, the electrolysis can be performed either for growing a thin film or to prepare large amounts of materials, i.e. at least 10 times more than on a standard platinum electrode.

3. Results

3.1. Dithiolene derivatives

The dithiolene complexes described here belong to various families of molecule-based materials: π donor–acceptor (DA) compounds, fractional oxidation state compounds (FOSC), and neutral compounds. Fig. 1 shows the structure

of the dithiolate ligands and donor molecules appearing in the examples.

3.1.1. $(NBu_4)_{0.9}[Ni(dmid)_2]$

To our knowledge, the FOSC $[NBu_4]_{0.9}[Ni(dmid)_2]$ is the first dithiolene-based material to be reported as grown as thin films [46]. Amorphous films having a thickness of 10 μm are electrochemically deposited, at 25 μA cm^{-2}, on Pt foils. The SEM micrograph of these films show a net-like or dendritic structure. The authors attribute this type of growth to the high currents applied during the film growth in favor of a large number of nuclei. A device could be built using these films and showed bi-stable electrical switching and memory phenomena [46].

3.1.2. $(NBu_4)_{0.29}[Ni(dmit)_2]$

The conductive $(NBu_4)_{0.29}[Ni(dmit)_2]$ phase is used in the fabrication of a thin film solid state device for the detection of gases at room temperature [56]. A gold interdigitated electrode system is applied. The film is grown at constant potential from a solution of the $(NBu_4)[Ni(dmit)_2]$ precursor in a 1:1 mixture of dichloromethane and nitrobenzene. The room-temperature conductivity of the film is 4×10^{-2} S cm^{-1} to be compared with the single crystal value of 10 S cm^{-1} [57]. The difference in conductivity between film and single crystal is consistent with the random orientation of crystallites within the film and the fact that $(NBu_4)_{0.29}[Ni(dmit)_2]$ exhibits an anisotropic conductive behavior, ratios in conductivity being $2:1:10^{-3}$ [57]. Nevertheless, the resistance of the film is sensitive to the presence of gases such as SO_2 and NO and decreases in both cases. In the presence of SO_2, the reduced $(NBu_4)[Ni(dmit)_2]$ species are produced, while in the presence of NO, oxidized $[Ni(dmit)_2]^0$ species are formed. Both species have lower conductivities than $(NBu_4)_{0.29}[Ni(dmit)_2]$ on single crystals, 3×10^{-8} and 3×10^{-3} S cm^{-1}, respectively [58]. Therefore, the resistance of the film increases when SO_2 and NO gases are detected. The authors report that when the sensor is submitted to SO_2 gas and further flushed with Ar, its resistance increases are reversible, while irreversibility is observed in the presence of NO [56]. The mechanism through which reversibility occurs is not explained by these authors. As Ar cannot oxidize the $(NBu_4)[Ni(dmit)_2]$ species back to the original FOSC one, the nature of the material present after Ar flush remains unknown.

3.1.3. $(NBu_4)_2[Ni(dcbdt)_2]_5$

Thin films of the FOSC $[NBu_4]_2[Ni(dcbdt)_2]_5$ phase are obtained by galvanostatic electrolysis of $[NBu_4][Ni(dcbdt)_2]$ on a silicon wafer in a one-compartment cell [59]. The oxidation is performed at room temperature and at a current density of 0.5 μA cm^{-2}. An ~10 μm continuous and adherent thin film is obtained after a 4 days electrolysis duration. Elemental analysis of a sample of film scratched from the surface confirms that the same 2:5 stoichiometry is obtained as on $[NBu_4]_2[Ni(dcbdt)_2]_5$ single crystals [60]. Electron micrographs demonstrate that the film is made up of thin elongated platelets (30–55 μm long, 1–8 μm width) randomly distributed on the substrate surface (Fig. 2).

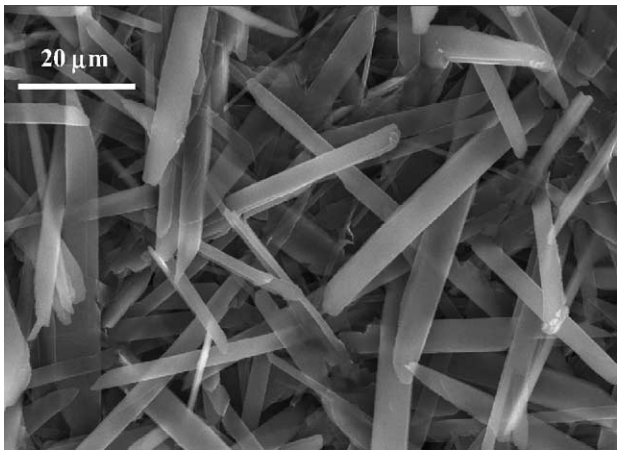

Fig. 2. SEM image of $[NBu_4]_2[Ni(dcbdt)_2]_5$ deposit on silicon.

The electrical conductivity of the films is about 1.2×10^{-2} S cm^{-1} at room temperature and follows a thermally activated semiconducting behavior identical to that reported for single crystals [61]. The room-temperature conductivity of the film is one order of magnitude lower than that of single crystals (0.15 S cm^{-1}). Within single crystals, the [−2 1 0] direction is the direction of highest conductivity. The contributions of other directions due the random orientation of the crystallites on the surface, and the polycrystalline nature of the film which generates grain boundaries, account for the lower conductivity value of the film versus that of the crystal. However, the conductivity ratio between single crystal and film is rather low and indicative of a more than one-dimensional system.

3.1.4. $TTF[Ni(dmit)_2]_2$

Electrodeposition of the π-DA $TTF[Ni(dmit)_2]_2$ phase is carried out on intrinsic Si(1 0 0) plates as anode and a platinum wire as cathode. The anodic oxidation of the TTF is performed at constant current density (1.5 μA cm^{-2}) at room temperature. Within 5 days, a black air-stable thin film is formed on the silicon electrode. When leaving the substrate for a longer time (>1 week) under the same conditions, thick (up to 300 μm) and still adhesive deposits suitable for conductivity measurements are obtained [62]. Scanning electron micrographs show a dense film made of roughly spherical grains with sizes ranging from 0.6 to 1 μm (Fig. 3) and EDS analysis confirms the presence of Ni and S elements. The observation of connected nano- or micrometer-size spheres, grown by a nucleation-coalescence mechanism, is commonly reported in electrochemical deposition processes [63].

Spectroscopic analyses (IR, Raman, XPS) are in agreement with those reported for $TTF[Ni(dmit)_2]_2$ single crystals. Furthermore, the Raman signal-to-noise ratio is as good as that of single crystals, confirming the good quality of the films, a crucial point for their potential applications in molec-

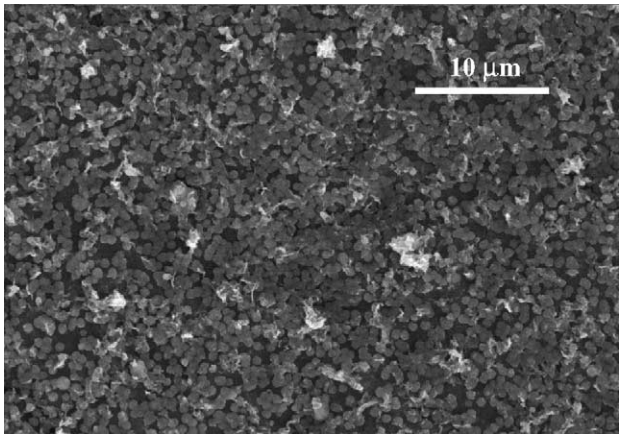

Fig. 3. SEM image of TTF[Ni(dmit)$_2$]$_2$ deposit on silicon.

ular electronic devices. Fig. 4 shows the electrical behavior of the electrodeposited material. Samples exhibit metallic behavior down to ca. 14 K, a temperature at which the resistance slightly increases. At 14 K, the resistance is around 4.3 times smaller than the resistance at 300 K, and is still 4 times smaller at 4.5 K. Such a behavior is reversible when warming back to room temperature, a reversibility is also observed on single crystals [13].

Taking into account the size and shape of the samples, the conductivity is ca. 12 S cm^{-1} at room temperature, and larger than 50 S cm^{-1} at 14 K. Obviously, these values are much lower than the values reported for the conductivities on single crystals (300 S cm^{-1} at 300 K, and 1.5×10^5 S cm^{-1} at 2 K). Nevertheless, whatever the substrate, due in part to grain boundaries and/or heterogeneous morphologies, the conductivity of thin films is usually very low and exhibits a semiconductive behavior. These TTF[Ni(dmit)$_2$]$_2$ films are the first example within the dithiolene family to display a metallic behavior down to very low temperature.

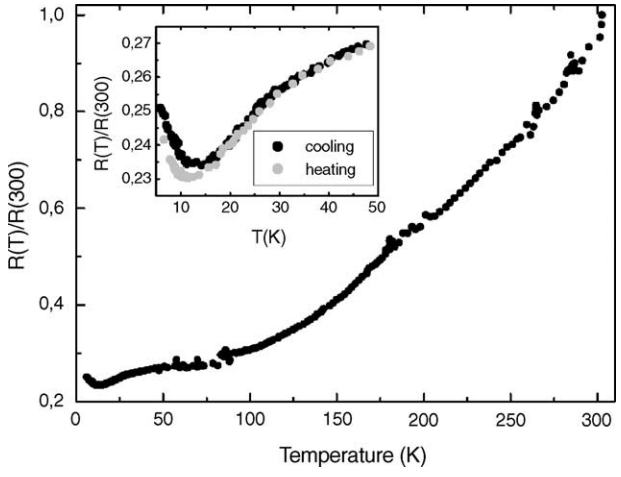

Fig. 4. Normalized resistance of a TTF[Ni(dmit)$_2$]$_2$ film as a function of temperature. Inset shows the low temperature region values for cooling (black dots) and heating (grey dots).

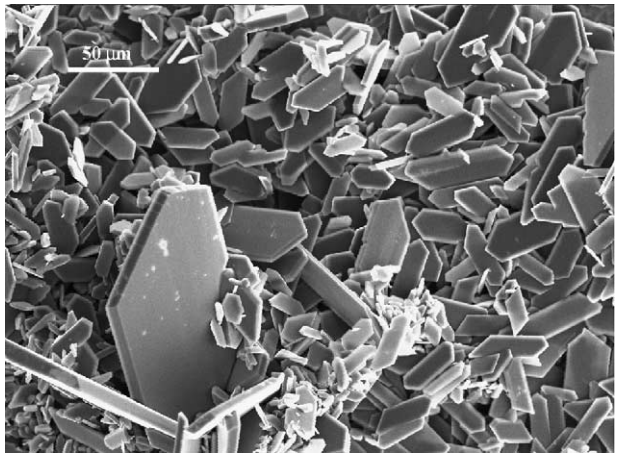

Fig. 5. SEM image of (BEDT-TTF)[Ni(dcbdt)$_2$] deposit on silicon.

3.1.5. *(BEDT-TTF)[Ni(dcbdt)$_2$]*

Efforts to prepare single crystals of the π-DA (BEDT-TTF)[Ni(dcbdt)$_2$] compound by conventional electrocrystallization were not successful. Using a Si(1 0 0) electrode as anode and galvanostatic oxidation (1 μA) of BEDT-TTF in the presence of NBu$_4$[Ni(dcbdt)$_2$], this phase could be isolated as a thin film [59]. Within 2 days, a black deposit (thickness ∼10 μm) is obtained on the silicon electrode. The composition, the microstructure and the spectroscopic data of the films remain unchanged after several months exposure to air. The deposit consists of faced microcrystals (size: 5–100 μm; thickness: 1–10 μm) uniformly covering the substrate surface (Fig. 5).

In addition to the crystalline deposit, single crystals grew on the edge of the substrate. One of these crystals was studied by X-ray diffraction, allowing the structure of the new phase to be determined. The compound is isostructural with previously described (BEDT-TTF)[Au(dcbdt)$_2$] [64] and can be regarded as BEDT-TTF containing layers alternating with [Ni(dcbdt)$_2$] containing ones along the [1 1 0] direction (Fig. 6).

The room-temperature conductivity, evaluated on a compressed pellet of the film collected from the silicon surface, is about 3×10^{-6} S cm^{-1}. This low value is similar to that obtained on (BEDT-TTF)[Au(dcbdt)$_2$] single crystals (<10^{-5} S cm^{-1}), and consistent with the structural arrangement of the compound [60].

3.1.6. *LB-[Au(dmtdt)$_2$] and LB-[M(dmit)$_2$], M = Au, Ni*

The application of the Langmuir–Blodgett technique is another way to organize molecule-based materials on surfaces [3]. A comprehensive review on electrically conductive LB-films has been published [65]. A more recent one reports on conductive and magnetic LB-systems [66]. A selection of transition metal-containing systems where preparation of the final material includes an electrochemical activation will be described herein. One of the characteristics of the LB-method is that it implies the use of precursors carrying long chain sub-

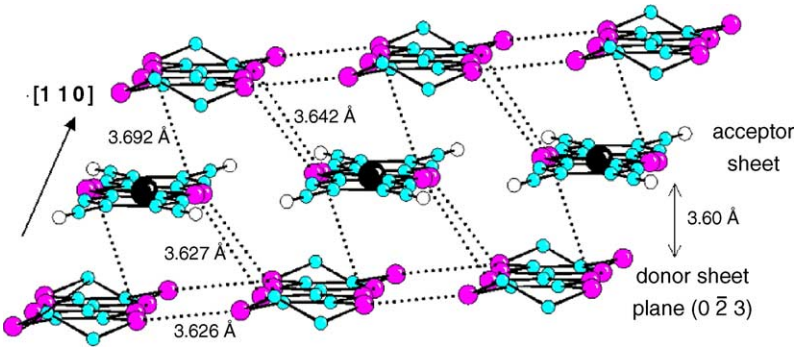

Fig. 6. Structural organization of donor and acceptor layers in (BEDT-TTF)[Ni(dcbdt)$_2$].

stituents. Therefore, the presence of such long chains modifies the interactions between the molecules in the solid state and may be accompanied with a drastic change of their physical properties. However, when the chains are located on part of the precursor to be eliminated under material formation, the final compound may be organized without modification of its properties. This strategy is applied to the preparation of films of the neutral systems [Au(dmtdt)$_2$] [50], [Ni(dmit)$_2$] [67,68], and [Au(dmit)$_2$] [51,69,70]. Typically, in a first step, LB-films of $3C_{10}$-Au(dmtdt)$_2$ or mC_n-M(dmit)$_2$ (M = Au, Ni) are prepared ($mC_n = (C_nH_{2n+1})_mN(CH_3)_{4-m}$ where $n = 10$, 14, 16, 18 and $m = 2$, 3). The "waiting time" defined as the time for which the starting compound is kept at the surface of the water is shown to be an important film-forming parameter in the case of LB-[Au(dmit)$_2$] [70]. In a second step, gold electrodes are evaporated on the films and used for electrochemical oxidation of the 1:1 LB-salts. The gold electrodes are sometimes formed on the substrate before LB-film formation [69]. In contrast to other examples described in this paper, the oxidation reaction takes place, not in solution, but within a supported phase. It operates on the gold complex molecules supported on the PET surface and imbedded in a cadmium stearate or an icosanoic acid layer, for the Au-tmdt and Au-dmit systems, respectively. The electrolysis is performed at constant current density, typically 0.1–0.2 μA cm^{-2} for 2–5 h and affords the LB-[Au(dmtdt)$_2$] and LB-[Au(dmit)$_2$] phases which no longer contain long chains. The gold electrodes are further used to measure the conductivity of the films. The conductivity of the LB-[Au(dmit)$_2$] films is reported to range from 0.1 to 40 S cm^{-1} at room temperature [51]. The $2C_{14}$-originating LB-[Au(dmit)$_2$] films are reported to be possibly superconductive at 3.9 K [71,72]. The $3C_{10}$-originating one exhibits a metallic conductivity down to 150 K [69]. The discrepancy observed in the room-temperature conductivity values is due to two features. The first one is the length of the alkyl chains of the ammonium cation which affects the molecular organization during LB-growth. As a matter of fact, the conductivity of the oxidized LB-[Au(dmit)$_2$] films decreases from 33 to 0.12 S cm^{-1} when the number of carbon atoms of the alkyl chain increases from 10 to 18 [69]. This feature is also reported for the conductivity of LB-[Ni(dmit)$_2$] films [67,68]. When the C_{10} precursor is considered, the discrepancy in conductivity values may be related to another feature, i.e. incomplete oxidation in some samples, which leads to a composite material associating neutral and 1:1 phases [51]. In the case of LB-[Au(dmtdt)$_2$], the authors mention that the oxidation of the 1:1 LB-salt partially occurs during film formation, because of the high reactivity of the monovalent ions towards oxygen. Further electrolysis is however necessary to complete the oxidation process and afford conductive films. Before electrolysis, the LB-[Au(dmtdt)$_2$] films are insulating. After electrolysis, they exhibit a conductivity of 1 S cm^{-1} at room temperature and a semiconductive behavior down to 110 K with an activation energy of 0.05 eV. Hückel molecular orbital calculations lead to the conclusion, based on the extended π-system afforded by the dmtdt ligand, that [Au(dmtdt)$_2$] LB-films have a chance to exhibit metallic conduction [50] as does the neutral Ni(tmdt)$_2$ phase which also exhibits an extended π-system [73]. Although this review focuses on electrochemically grown films, a field effect transistor (FET) device can be produced using LB-layers of (*N*-octadecylpyridinium)[Ni(dmit)$_2$] chemically doped through exposition to iodine vapor [74]. Also, within the field of sensors, LB-films of bis[(4-diethylamino)dithiobenzyl]nickel are very efficient for the detection of hydrazine in the gas phase [75]. The conductivity of the films is sensitive to 0.5 ppm of this compound in the gas phase at room temperature [76,77].

3.1.7. *[M(dmit)$_2$], M = Ni, Pd*

$(1C_{15})_2$[Ni(dmit)$_2$] is electrolyzed on ITO glass slices at constant potential and affords the FOSC $(1C_{15})_x$[Ni(dmit)$_2$] phase as a film. In this case, no previous LB-deposition is performed. By further covering the film with an aluminum layer, an electrical memory switching system exhibiting bi-stability can be built [53,54]. Another type of FOSC films is obtained from the galvanostatic electrolysis of a [M(dmit)$_2$] salt containing a polymeric cation, i.e. (PVOP)$_2$[M(dmit)$_2$] with M = Ni and Pd and PVOP = poly(4-vinyl-*N*-octanylpyridinium)[52]. Copper substrates are used as anodes. A copper layer is further evaporated on the film for 2-probe conductivity measurements within the thickness. The room-temperature conductivity of the films of both Ni and Pd derivatives is about 10^{-4} S cm^{-1}.

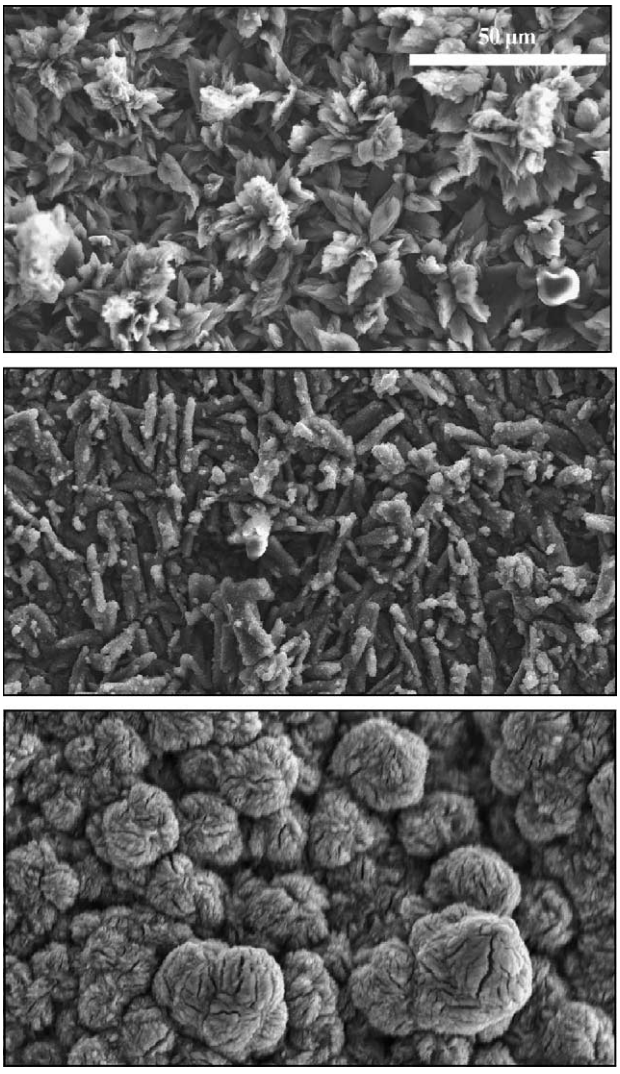

Fig. 7. SEM images of $[Ni(tmdt)_2]$ deposits on silicon. Scale bar applies to all images. Top: 2.5 μA cm^{-2}, 5 days. Middle: 1.1 μA cm^{-2}, 12 days. Bottom: 1.4 μA cm^{-2}, 19 days.

3.1.8. $[Ni(tmdt)_2]$

This neutral compound exhibits a metallic conductivity. At room temperature, the conductivity of single crystals is 400 S cm^{-1} [73]. Thin films are grown on silicon substrates from acetonitrile solutions of $(NMe_4)_2[Ni(tmdt)_2]$ by the galvanostatic technique [78]. Typically, current densities ranging from 1.1 to 2.5 μA cm^{-2} are applied for 5–20 days, while the solution is heated at 30 °C. Depending on these conditions, various crystal shapes, flakes, rods or spherical grains, are observed within the crystalline films (Fig. 7). The silicon wafer is uniformly covered with the deposit. The thickness of the deposits goes from 4 μm (top film) to 25 μm (bottom film).

The results of IR, Raman and XPS studies of the deposits are consistent with the formation of the neutral $[Ni(tmdt)_2]$ phase. XRD performed on the deposit indicates that the structure of the compound is identical to that of single crystals. Four-probe conductivity measurements give room-temperature values ranging from 1 to 30 S cm^{-1} to be compared with 400 S cm^{-1} on single crystals. The existence of resistive grain boundaries forbids metallic behavior within the films. However, very low activation energies are measured, i.e. a few meV.

3.2. Prussian blue and chromium analogues

3.2.1. Prussian blue $Fe^{III}_4[Fe^{II}(CN)_6]_3$

Epitaxial Prussian blue (PB) thin films grow on single-crystal Au(1 1 0) substrates [47]. Growth of the PB film is performed according to [79], by applying a constant potential (+0.3 V versus SCE) to the gold substrate electrode for 1 h at room temperature. The reference electrode is SCE and a Pt wire acts as counter electrode. The electrolytic solution consists of $K_3[Fe(CN)_6]$ and $[Fe(NO_3)_3]$ salts dissolved in a KCl supporting electrolyte solution prepared in water. The films are perfectly continuous and appear as aligned pyramidal structures on the surface.

A recent review describes the electrosynthesis, in situ characterization, and applications of other metal hexacyanoferrates (metal = Cu, Pd, In, V, Co, and Ni) [80]. Potentiodynamic cycling is performed between pre-set potential limits of the working electrode placed in a supporting electrolyte containing the metal ion and ferricyanide species. A metal-active electrode can be used for copper and nickel analogues [81]. In other cases, inert electrodes (glassy carbon, graphite, Pt or Au) are used and the metal ions are added to the electrolytic solution. When optical applications are envisioned, transparent conducting electrodes are used, such as tin-doped indium oxide (ITO) or fluorine-doped tin oxide glass. Display windows, photoimaging, biological sensing, magneto-optic switching are among the described examples of devices using metal hexacyanoferrates thin films.

3.2.2. Chromium analogues of Prussian blue

Mixed valence chromium cyanides which are PB analogues are grown as thin films on a SnO_2 working electrode [48]. Depending on the conditions, the stoichiometry of the product varies. Thin films of various colors are obtained depending on the electrode potential. Ferrimagnetic thin films with high T_c values are produced. The highest $T_c = 270$ K is obtained for $Cr_{2.12}(CN)_6$. The T_c of the systems can be tuned by varying the electrochemical conditions. When the magnetic films are used as electrodes and biased from −1.2 to −1.0 V versus SCE in a KCl aqueous solution, redox reactions occur and are accompanied with changes of color and magnetic properties. Upon this type of electrochemical activation, a reversible shift of T_c is demonstrated, the corresponding cyanide being switched reversibly back and forth between ferrimagnetism and paramagnetism. Thin films (1–2 μm thick) of amorphous and crystalline form of $K_nCr_x[Cr(CN)_6]$ are electrodeposited on glassy carbon or ITO electrodes [49]. Reactants are $CrCl_3$, $K_3Cr(CN)_6$ in KCl aqueous solution. Films exhibiting various grain-like morphologies (balls or cubes) are obtained by cycling the po-

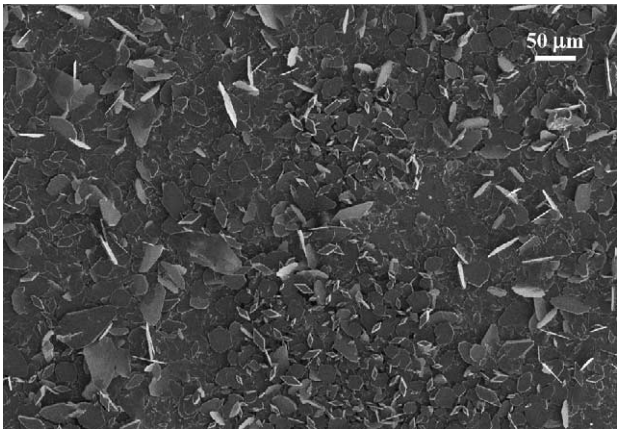

Fig. 8. SEM image of θ-$(BETS)_4[Fe(CN)_5NO]$ deposit on silicon.

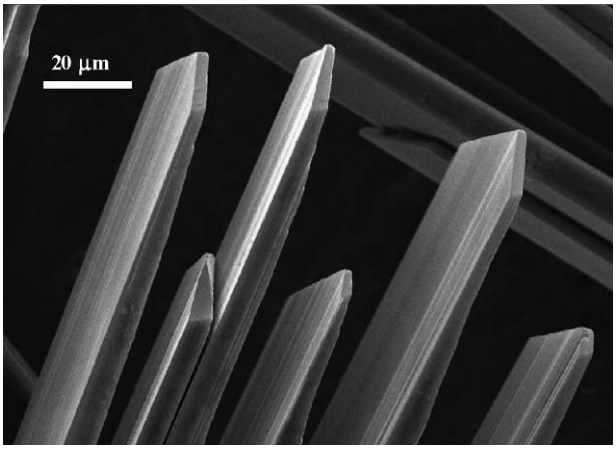

Fig. 9. SEM image of $(BEDT\text{-}TTF)_4K[Fe(CN)_5NO]_2$ deposit on silicon.

tential of the working electrode 5–10 times between −0.2 and −1.0 V. The magnetization data reveal magnetic ordering with a T_c as high as 260 K and hysteresis.

3.3. Nitroprusside compounds and ruthenium analogues

3.3.1. θ-$(BETS)_4[Fe(CN)_5NO]$ and $(BEDT\text{-}TTF)_4K[Fe(CN)_5NO]_2$

Electrodeposition using a 2 in. Si(1 0 0) wafer as anode and a platinum wire as counter electrode leads to the growth of thin films of the θ-$(BETS)_4[Fe(CN)_5NO]$ phase [55]. Oxidation of the BETS donor molecule is performed under galvanostatic conditions (0.1 μA cm^{-2}) at room temperature in the presence of $(Ph_4P)_2[Fe(CN)_5NO]$. The θ-$(BETS)_4[Fe(CN)_5NO]$ phase may exhibit coupled conductive and photochromic properties. SEM images (Fig. 8) show that the deposit uniformly covers the surface of the substrate. The film contains platelets of irregular shapes but also diamond- and hexagonal-shaped single crystals.

The conductivity of the film is about 1.6 S cm^{-1} at room temperature. This high value compared to 10^{-2} S cm^{-1} obtained on single crystal shows the high intrinsic conductivity of the material. Despite the low conductivity of inter-grain contacts within the film, the two orders of magnitude observed between the crystal and the film is attributed to the fact that the measurement on single crystal was not performed along the most favorable conductive direction, because the shape and size of the crystal did not allow another orientation [32]. Moreover, the semiconductive thermal behavior (E_a = 0.03 eV) compared to the metallic one observed for the single crystal means that the overall electric behavior of the material is somewhat affected by the inter-grain contacts.

Similarly, $(BEDT\text{-}TTF)_4K[Fe(CN)_5NO]$ films are obtained from the oxidation of the BEDT-TTF donor in the presence of $K_2[Fe(CN)_5NO]$. As shown on Fig. 9, films consist of long needles, a crystallite morphology similar to that of single crystals previously prepared [27].

The conductivity of the film is 3.5 S cm^{-1}, a value very close to that of single crystals (14 S cm^{-1}). Moreover, the semiconductive behavior of the film is accompanied with a very low activation energy (E_a = 0.006 eV). Let us recall that single crystals of this phase are metallic. The photochromic properties of θ-$(BETS)_4[Fe(CN)_5NO]$ and $(BEDT\text{-}TTF)_4K[Fe(CN)_5NO]_2$ films are currently under investigation.

3.3.2. $(BETS)_2[RuX_5NO]$, X = Cl, Br

The electrochemical oxidation of BETS in the presence of $K_2[RuX_5NO]$ is performed on Si(1 0 0) substrates in a H-type cell. The counter electrode is a Pt wire and galvanostatic electrolysis is applied at room temperature using a current density of 0.2 and 0.9 μA cm^{-2} for X = Cl and Br, respectively. SEM images show that the deposits consist of thick grain like platelets in the case of Cl derivative. Needles are observed in addition to grains in the case of the Br derivative. The two compounds are known to exhibit different conductive properties [32]. A comparative study of their XRD structures and of the Raman data obtained from the films demonstrates a different charge transfer between the BETS moiety and the $[RuCl_5NO]$ or $[RuBr_5NO]$ species. In the insulating Cl derivative, the charge transfer is found to be 1, while in the semiconductive Br derivative results indicate that it is different from 1 and approaches 0.9 [82]. These values of charge transfer are in agreement with the conductive properties of both compounds.

3.4. Polyoxometalate derivatives

Polyoxometalates (POMs) are of interest to build up organic/inorganic hybrid materials displaying multiple physical properties. POM-containing conductive phases have been prepared with TTF-like donors [40,41]. Polymer-POM composite films have been reported with a large variety of different polymers [83–87]. POM-based materials have also been obtained as LB-films [88,89], however, as no electrochemical activation is involved in the preparation of these films, they will not be described here. Other combinations of conductive polymers with different inorganic species but POMs or tran-

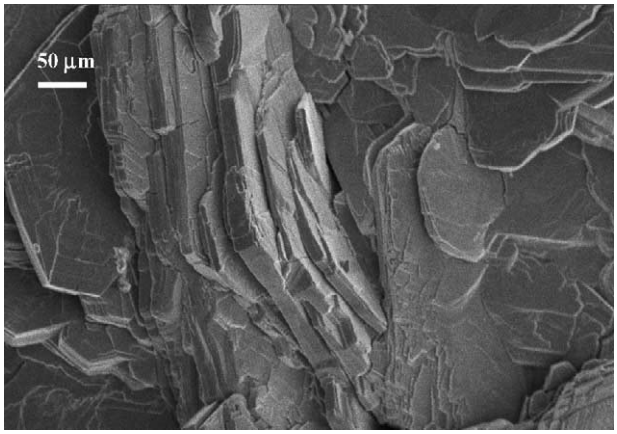

Fig. 10. SEM image of $(TTF)_6[N(C_2H_5)_4]H(PW_{12}O_{40})$ deposit on silicon.

sition metal complexes, relate to the huge field of modified electrodes and will not be reviewed either.

3.4.1. TTF[polyoxometalate]

TTF-POMs films can be grown by galvanostatic electrolysis (1 μA) at room temperature using a H-type cell equipped with a Si anode (1 cm × 1 cm) and a Pt wire counter electrode. Oxidation of TTF, in acetonitrile and in the presence of $[N(C_2H_5)_4]_3(PW_{12}O_{40})$ leads to a black amorphous thin film (no XRD lines). SEM images (Fig. 10) demonstrate a film made of stacked sheets, with an individual thickness ranging from 5 to 25 μm.

XPS reveals a S/W ratio of 1.92 in agreement with a 6 TTF/1 $PW_{12}O_{40}$ stoichiometry (S/W = 2), as in $(TTF)_6[N(C_2H_5)_4](H)(PW_{12}O_{40})$ single crystals grown on a Pt anode [90]. The IR spectrum is similar to that of $(TTF)_6[N(C_2H_5)_4](H)(PW_{12}O_{40})$. The room-temperature conductivity of the powder collected from the substrate surface is $\approx 2 \times 10^{-5}$ S cm^{-1}, to be compared with $\approx 10^{-3}$ S cm^{-1} on single crystals. From the magnetic studies, an effective moment of 1.5 μ_B (RT) is obtained, identical to that of single crystals.

3.4.2. Polymer-polyoxometalate composites

Within the polymer-POM composites, the POM inorganic anions are embedded within the polymer matrix. Polypyrrole (Ppy) systems are electrochemically produced at constant potential on the electrode surface (Pt foil) in the presence of the POM units acting as supporting electrolytes [85,86]. Ppy-POM films show semiconductive properties and a wide range of room-temperature conductivities ranging from 0.1 S cm^{-1} for the Ppy-$[Co_4(H_2O)_2(PW_9O_{34})_2]^{10-}$ composite [87] to 225 S cm^{-1} for the Ppy-$[CrMo_6O_{24}H_6]^{3-}$ one [85]. In the Ppy-$[Co_4(H_2O)_2(PW_9O_{34})_2]^{10-}$ composite, the magnetic properties of the ferromagnetic cobalt cluster remains. This composite was the first hybrid film formed from a high spin cluster embedded in a polypyrrole matrix.

4. Conclusion

This review highlighted the preparation as thin films of transition metal-containing molecule-based materials. The electrodeposition method was considered and can be applied to all systems where the precursors are soluble and lead to the final material through an electrochemical activation. Within the dithiolato-bearing complexes, we have seen with $TTF[Ni(dmit)_2]_2$ that, although films exhibit a polycrystalline morphology, they show metal-like behavior. In the case of $[Ni(dcbdt)_2]$ derivatives, the electrodeposition method allowed us to isolate the (BEDT-TTF)$[Ni(dcbdt)_2]$ while standard electrocrystallization was not successful. In the compounds described, the properties observed with single crystals are generally transferred to the film and only influenced by its polycrystalline character. However, the orientation and the two-dimensional growth of the film on the silicon surface, played in favor of better conductive properties in the case of the θ-$(BETS)_4[Fe(CN)_5NO]$ compound. Neutral materials such as $[Au(tmdt)_2]$, $[Au(dmit)_2]$ and $[Ni(tmdt)_2]$ are also deposited as thin films. Note that the first two are prepared from LB-salts in which the long chains do not influence the material properties as they remain in the counter-ion after electrolysis. The thin film morphology does not modify either the magnetic properties of Prussian blue and its chromium analogues. In the domain of photochromic anion-containing systems, the use of film samples allowed us to undertake useful Raman studies, for example of $(BETS)_2[RuBr_5NO]$ and $(BETS)_2[RuCl_5NO]$, from which a better understanding of the conductive property difference between these two phases was obtained. Finally, the use of silicon wafers has been largely shown in the selected examples. This substrate is particularly interesting for electronic applications. Note also that, apart from the film growth, the use of an entire 2 in. silicon wafer, a much cheaper substrate than a gold or platinum electrode of the same surface area, allows one to prepare large amounts of product, i.e. 60–80 mg versus 10–20 crystals with the standard electrocrystallization conducted on a Pt wire electrode. Film deposition studies of molecule-based materials are key steps to the application of these materials in devices. Electrodeposition is one of the methods that can be applied. Vapor phase methods, LB-technique, drop casting, spin or dip coating, stamping and ink-jet printing are also to be considered. A combination of various methods may allow the formation of multi-layer structures. The preparation of LB-$[Au(tmdt)_2]$ and LB-$[Au(dmit)_2]$ films is an example of such a possibility.

Acknowledgement

Part of the work described here is issuing from the "Molecules and Materials" team and has been carried out with financial support of various institutions and programs: CNRS PICS and PAI, COST D14, INTAS, Marie Curie fellowships and ATUPS from Université Paul Sabatier. The

authors thank the contribution and collaboration of the following persons: M. Almeida (dcbdt-complexes), M.-L. Doublet (calculations), J.-M. Fabre (tmdt precursor), J. Fraxedas (XPS), L. Ouahab (polyoxometalates), F. Senocq (XRD), A. Zwick (Raman), V. Collière (SEM/EDX), A. Mari and J.-F. Meunier (SQUID) and all students and post-doctorates having been involved.

References

[1] R.M. Metzger, in: L. Ouahab, E.B. Yagubskii (Eds.), Organic Conductors, Superconductors and Magnets: From synthesis to Molecular Electronics, NATO Science Series II. Mathematics, Physics and Chemistry, vol. 139, Kluwer Academic and NATO Scientific Affairs Division, Dordrecht/Boston/London, 2004, p. 269.
[2] D.L. Allara, C. McGuiness, R.M. Metzger, in: L. Ouahab, E.B. Yagubskii (Eds.), Organic Conductors, Superconductors and Magnets: From synthesis to Molecular Electronics, NATO Science Series II. Mathematics, Physics and Chemistry, vol. 139, Kluwer Academic and NATO Scientific Affairs Division, Dordrecht/Boston/London, 2004, p. 295.
[3] P. Delhaes, in: L. Ouahab, E.B. Yagubskii (Eds.), Organic Conductors, Superconductors and Magnets: From synthesis to Molecular Electronics, NATO Science Series II. Mathematics, Physics and Chemistry, vol. 139, Kluwer Academic and NATO Scientific Affairs Division, Dordrecht/Boston/London, 2004, p. 217.
[4] U. Geiser, H.H. Wang, C.Y. Han, G.A. Willing, in: L. Ouahab, E.B. Yagubskii (Eds.), Organic Conductors, Superconductors and Magnets: From synthesis to Molecular Electronics, NATO Science Series II. Mathematics, Physics and Chemistry, vol. 139, Kluwer Academic and NATO Scientific Affairs Division, Dordrecht/Boston/London, 2004, p. 231.
[5] N.L. Rosi, C.A. Mirkin, Chem. Rev. 105 (2005) 1547.
[6] J.C. Love, L.A. Estroff, J.K. Kriebel, R.G. Nuzzo, G.M. Whitesides, Chem. Rev. 1005 (2005) 1103.
[7] L. Valade, D. de Caro, I. Malfant, in: L. Ouahab, E.B. Yagubskii (Eds.), Organic Conductors, Superconductors and Magnets: From synthesis to Molecular Electronics, NATO Science Series II. Mathematics, Physics and Chemistry, vol. 139, Kluwer Academic and NATO Scientific Affairs Division, Dordrecht/Boston/London, 2004, p. 241.
[8] T.W. Kelley, P.F. Baude, C. Gerlach, D.E. Ender, D. Muyres, M.A. Haase, D.E. Vogel, S.D. Theiss, Chem. Mater. 16 (2004) 4413.
[9] D. De Caro, M. Basso-Bert, J. Sakah, H. Casellas, J.-P. Legros, L. Valade, P. Cassoux, Chem. Mater. 12 (2000) 587.
[10] H. Casellas, D. De Caro, L. Valade, P. Cassoux, Chem. Vap. Dep. 8 (2002) 145.
[11] E. Lamouroux, E. Alric, H. Casellas, L. Valade, D. De Caro, M. Etienne, D. Gatteschi, Electrochem. Soc. Proc. 8 (2003) 1040.
[12] E. Lamouroux, D. De Caro, L. Valade, Thin Solid Films 467 (2004) 93.
[13] M. Bousseau, L. Valade, J.-P. Legros, P. Cassoux, M. Garbauskas, L.V. Interrante, J. Am. Chem. Soc. 108 (1986) 1908.
[14] L. Brossard, M. Ribault, M. Bousseau, P. Valade, P. Cassoux, C.R. Acad. Sci. Paris 302-II (1986) 205.
[15] A. Kobayashi, E. Fujiwara, H. Kobayashi, Chem. Rev. 104 (2004) 5243.
[16] M. Fourmigué, Acc. Chem. Res. 37 (2004) 179.
[17] A. Kobayashi, H. Kobayashi, Charge Transfer Salts, Fullerenes and Photoconductors in: H.S. Nalwa (Ed.), Handbook of Conductive Molecules and Polymers, vol. 1, Wiley, Chichester, 1997, p. 249.
[18] G.C. Papavassiliou, A. Terzis, P. Delhaes, Charge Transfer Salts, Fullerenes and Photoconductors in: H.S. Nalwa (Ed.), Handbook of Conductive Molecules and Polymers, vol. 1, Wiley, Chichester, 1997, p. 151.
[19] J.S. Miller, J.C. Calabrese, H. Rommelmann, S.R. Chittipeddi, J.H. Zhang, W.M. Reiff, A.J. Epstein, J. Am. Chem. Soc. 109 (1987) 769.
[20] C. Faulmann, E. Rivière, S. Dorbes, F. Senocq, E. Coronado, P. Cassoux, Eur. J. Inorg. Chem. (2003) 2880.
[21] E. Coronado, P. Day, Chem. Rev. 104 (2004) 5419.
[22] T. Enoki, A. Miyazaki, Chem. Rev. 104 (2004) 5449.
[23] M. Kurmoo, A.W. Graham, P. Day, S.J. Coles, M.B. Hursthouse, J.M. Caulfield, J. Singleton, L. Ducasse, P. Guionneau, J. Am. Chem. Soc. 117 (1995) 12209.
[24] E. Coronado, J.R. Galan-Mascaros, C.J. Gomez-Garcia, V. Laukhin, Nature 408 (2000) 447.
[25] A. Alberola, E. Coronado, J.R. Galan-Mascaros, C. Gimenez-Saiz, C.J. Gomez-Garcia, J. Am. Chem. Soc. 125 (2003) 10774.
[26] H. Kobayashi, A. Kobayashi, P. Cassoux, Chem. Soc. Rev. 29 (2000) 325.
[27] L.A. Kushch, L. Buravov, V. Tkatcheva, E.B. Yagubskii, L.V. Zorina, S.S. Khasanov, R.P. Shibaeva, Synt. Met. 102 (1999) 1646.
[28] M. Gener, E. Canadell, S.S. Khasanov, L.V. Zorina, R.P. Shibaeva, L.A. Kushch, E.B. Yagubskii, Solid-State Commun. 111 (1999) 329.
[29] L.V. Zorina, S.S. Khasanov, R.P. Shibaeva, M. Gener, R. Rousseau, E. Canadell, L.A. Kushch, E.B. Yaguskii, O.O. Drozdova, K. Yakushi, J. Mater. Chem. 10 (2000) 2017.
[30] M. Clemente-León, E. Coronado, J.R. Galan-Mascaros, C.J. Gomez-Garcia, E. Canadell, Inorg. Chem. 39 (2000) 5394.
[31] M. Clemente-León, E. Coronado, J.R. Galan-Mascaros, C. Gimenez-Saiz, C.J. Gomez-Garcia, E. Ribera, J. Vidal-Gancedo, C. Rovira, E. Canadell, V. Laukhin, Inorg. Chem. 40 (2001) 3526.
[32] M.-E. Sanchez, M.-L. Doublet, C. Faulmann, I. Malfant, P. Cassoux, L.A. Kushch, E.B. Yagubskii, Eur. J. Inorg. Chem. (2001) 2797.
[33] K.N. Houk, H. Kessler, J.-M. Lehn, S.V. Ley, A. de Meijere, S.L. Schreiber, J. Thiem, B.M. Trost, F. Vögtle, H. Yamamoto (Eds.), Spin Crossover in Transition Metal Compounds IP. Gütlich, H.A. Goodwin (Eds.), Top. Curr. Chem., vol. 233, Springer, Heidelberg, 2004.
[34] K.N. Houk, H. Kessler, J.-M. Lehn, S.V. Ley, A. de Meijere, S.L. Schreiber, J. Thiem, B.M. Trost, F. Vögtle, H. Yamamoto (Eds.), Spin Crossover in Transition Metal Compounds IIP. Gütlich, H.A. Goodwin (Eds.), Top. Curr. Chem., vol. 234, Springer, Heidelberg, 2004.
[35] K.N. Houk, H. Kessler, J.-M. Lehn, S.V. Ley, A. de Meijere, S.L. Schreiber, J. Thiem, B.M. Trost, F. Vögtle, H. Yamamoto (Eds.), Spin Crossover in Transition Metal Compounds IIIP. Gütlich, H.A. Goodwin (Eds.), Top. Curr. Chem., vol. 235, Springer, Heidelberg, 2004.
[36] J.S. Miller, Electrochem. Soc. Interface 11 (2002) 22.
[37] M. Verdaguer, N. Galvez, R. Garde, C. Desplanches, Electrochem. Soc. Interface 11 (2002) 28.
[38] S. Ohkoshi, K. Hashimoto, Electrochem. Soc. Interface 11 (2002) 34.
[39] S. Ferlay, T. Mallah, R. Ouahès, P. Veillet, M. Verdaguer, Nature 378 (1995) 701.
[40] E. Coronado, C.J. Gomez-Garcia, Chem. Rev. 98 (1998) 273.
[41] L. Ouahab, C.R. Acad. Sci. Paris IIc (1986) 205.
[42] C. Faulmann, P. Cassoux, in: E.I. Stiefel (Ed.), Dithiolene Chemistry. Synthesis, Properties, and Applications in: K.D. Karlin (Ed.), Progress in Inorganic Chemistry, 52, Wiley, Hoboken, NJ, 2004, p. 399.
[43] N. Robertson, L. Cronin, Coord. Chem. Rev. 227 (2002) 93.
[44] R. Kato, Chem. Rev. 104 (2004) 5319.
[45] P. Cassoux, L. Valade, P.-L. Fabre, in: A.B.P. Lever (Ed.), Fundamentals: Ligands, Complexes, Synthesis, Purification and Structure in: J.A. McCleverty, T.J. Meyer (Eds.), Comprehensive Coordination Chemistry II: From Biology to Nanotechnology, vol. 1, Elsevier, Amsterdam, 2003, p. 761.

[46] S.G. Liu, P.J. Wu, Y.Q. Liu, D.B. Zhu, Mol. Cryst. Liq. Cryst. 275 (1996) 211.
[47] S. Nakanishi, G. Lu, H.M. Kothari, E.W. Bohannan, J.A. Switzer, J. Am. Chem. Soc. 125 (2003) 14998.
[48] O. Sato, T. Iyoda, A. Fujishima, K. Hashimoto, Science 271 (1996) 49.
[49] W.E. Buschmann, S.C. Paulson, C.M. Wynn, M.A. Girtu, A.J. Epstein, H.S. White, J.S. Miller, Chem. Mater. 10 (1998) 1386.
[50] T. Takahashi, K. Sakai, T. Yumoto, T. Akutagawa, T. Hasegawa, T. Nakamura, Thin Solid Films 393 (2001) 7.
[51] H. Isolato, J. Paloheimo, Y.F. Miura, R. Azumi, M. Matsumoto, T. Nakamura, Phys. Rev. B 51 (1995) 1809.
[52] R. Shen, W. Xu, D. Zhang, D. Zhu, Solid-State Commun. 130 (2004) 401.
[53] M.Y. Han, W. Huang, Mater. Chem. Phys. 49 (1997) 179.
[54] M.Y. Han, W. Huang, D. Zhang, T.J. Li, Chem. Lett. (1997) 43.
[55] L. Pilia, I. Malfant, D. De Caro, F. Senocq, A. Zwick, L. Valade, New J. Chem. 28 (2004) 52.
[56] J.R. Bates, P. Kathirgamanathan, R.W. Miles, Electron. Lett. 31 (1995) 1225.
[57] L. Valade, M. Bousseau, A. Gleizes, P. Cassoux, J. Chem. Soc., Chem. Commun. (1983) 110.
[58] P. Cassoux, L. Valade, H. Kobayashi, R. Clark, A.E. Underhill, Coord. Chem. Rev. 110 (1991) 115.
[59] D. De Caro, H. Alves, M. Almeida, S. Caillieux, M. Elgaddari, C. Faulmann, I. Malfant, F. Senocq, J. Fraxedas, A. Zwick, L. Valade, J. Mater. Chem. 14 (2004) 2801.
[60] H. Alves, D. Simao, I.C. Santos, E.B. Lopes, H. Novais, R.T. Henriques, M. Almeida, Synt. Met. 135 (2003) 543.
[61] D. Simao, H. Alves, D. Belo, S. Rabaca, E.B. Lopes, I.C. Santos, V. Gama, M.T. Duarte, R.T. Henriques, H. Novais, M. Almeida, Eur. J. Inorg. Chem. (2001) 3119.
[62] D. De Caro, J. Fraxedas, C. Faulmann, I. Malfant, J. Milon, J.-F. Lamère, V. Collière, L. Valade, Adv. Mater. 16 (2004) 835.
[63] M. Paunovic, M. Schlesinger, Fundamentals of Electrochemical Deposition, Wiley, New York, 1998.
[64] H. Alves, D. Simao, I.C. Santos, V. Gama, R.T. Henriques, H. Novais, M. Almeida, Eur. J. Inorg. Chem. (2004) 1318.
[65] T. Nakamura, Charge Transfer Salts, Fullerenes and Photoconductors in: H.S. Nalwa (Ed.), Handbook of Conductive Molecules and Polymers, vol. 1, Wiley, Chichester, 1997, p. 727.
[66] D.R. Talham, Chem. Rev. 104 (2004) 5479.
[67] T. Nakamura, H. Tanaka, M. Matsumoto, H. Tashibana, E. Manda, Y. Kawabata, Synt. Met. 27 (1988) 601.
[68] T. Nakamura, H. Tanaka, M. Matsumoto, H. Tashibana, E. Manda, Y. Kawabata, Chem. Lett. (1988) 1667.
[69] T. Nakamura, Y. Miura, M. Matsumoto, H. Tashibana, M. Tanaka, Y. Kawabata, in: G. Saito, S. Kagoshima (Eds.), The Physics and Chemistry of Organic Superconductors, Springer Proceedings in Physics, 51, Springer-Verlag, Berlin/Heidelberg, 1990, p. 424.
[70] M. Horikiri, Y. Araki, K. Ikegami, Y.F. Miura, M. Sugi, Synt. Met. 133 (2003) 665.
[71] Y.F. Miura, M. Horikiri, S. Tajima, T. Wakaita, S. Saito, M. Sugi, Synt. Met. 120 (2001) 727.
[72] Y.F. Miura, M. Horikiri, S. Tajima, T. Wakaita, S.H. Saito, M. Sugi, Synt. Met. 133 (2003) 663.
[73] H. Tanaka, Y. Okano, H. Kobayashi, W. Suzuki, A. Kobayashi, Science 291 (2001) 285.
[74] C. Pearson, J.E. Gybson, A.J. Moore, M.R. Bryce, M.C. Petty, Electron. Lett. 29 (1993) 1377.
[75] J.W. Grate, S. Rose-Pehrson, W.R. Barger, Langmuir 4 (1988) 1293.
[76] D.-Q. Yang, R.-F. Wang, S.-P. Xie, Y. Guo, Proc. SPIE, Int. Soc. Opt. Eng. 3175 (1998) 82.
[77] D.-Q. Yang, Y. Sun, S.-P. Xie, R.-F. Wang, Y. Guo, C.-Z. Fan, D.-A. Da, Thin Solid Films 320 (1998) 316.
[78] K. Rivasseau, Report, Université Paul Sabatier, Toulouse III and ENSIACET, Toulouse, 2004.
[79] K. Itaya, I. Uchida, V.D. Neff, Acc. Chem. Res. 19 (1986) 162.
[80] N.R. de Tacconi, K. Rajeshwar, R.O. Lezna, Chem. Mater. 15 (2003) 3046.
[81] S. Zamponi, M. Berrettoni, P.J. Kulesza, K. Miecznikowski, M.A. Malik, O. Makowski, R. Marassi, Electrochim. Acta 48 (2003) 4261.
[82] I. Malfant, A. Glaria, J.-F. Lamère, B. Garreau De Bonneval, D. de Caro, L. Valade, M.-L. Doublet, A. Zwick, Manuscript, unpublished results.
[83] M. Lira-Cantu, P. Gomez-Romero, Chem. Mater. 10 (1998) 698.
[84] P. Gómez-Romero, M. Lira-Cantú, Adv. Mater. 9 (1997) 144.
[85] T.F. Otero, S.A. Cheng, E. Coronado, E.M. Ferrero, C.J. Gomez-Garcia, Chem. Phys. Chem. 3 (2002) 808.
[86] S. Cheng, T. Fernandez-Otero, E. Coronado, C.J. Gomez-Garcia, E. Martinez-Ferrero, C. Gimenez-Saiz, J. Phys. Chem. B 106 (2002) 7585.
[87] M. Clemente-Leon, E. Coronado, J.R. Galan-Mascaros, C. Gimenez-Saiz, C.J. Gomez-Garcia, T. Fernandez-Otero, J. Mater. Chem. 8 (1998) 309.
[88] M. Clemente-Leon, B. Agricole, C. Mingotaud, C.J. Gomez-Garcia, E. Coronado, P. Delhaes, Angew. Chem., Int. Ed. Engl. 36 (1997) 1114.
[89] M. Clemente-Leon, B. Agricole, C. Mingotaud, C.J. Gomez-Garcia, E. Coronado, P. Delhaes, Langmuir 13 (1997) 2340.
[90] L. Ouahab, M. Bencharif, A. Mhanni, D. Pelloquin, J.-F. Halet, O. Peña, J. Padiou, D. Grandjean, C. Garrigou-Lagrange, J. Amiell, P. Delhaes, Chem. Mater. 4 (1992) 666.